Reversed Conductance Decay of 1D Topological Insulators by Tight-Binding Analysis

Liang Li[a], Suman Gunasekaran*[b], Yujing Wei[a], Colin Nuckolls[a], Latha Venkataraman*[a,c]

[a]Department of Chemistry, Columbia University, New York, New York 10027, United States

[b]Department of Chemistry and Chemical Biology, Cornell University, Ithaca, New York 14853, United States

[c]Department of Applied Physics and Applied Mathematics, Columbia University, New York, New York 10027, United States

Email: sg875@cornell.edu, lv2117@columbia.edu

ABSTRACT: Reversed conductance decay describes increasing conductance of a molecular chain series with increasing chain length. Realizing reversed conductance decay is an important step towards making long and highly conducting molecular wires. Recent work has shown that one-dimensional topological insulators (1D TIs) can exhibit reversed conductance decay due to their non-trivial edge states. The Su-Schrieffer-Heeger (SSH) model for 1D TIs relates to the electronic structure of these isolated molecules but not their electron transport properties as single-molecule junctions. Herein, we use a tight-binding approach to demonstrate that polyacetylene and other diradicaloid 1D TIs show a reversed conductance decay at the short chain limit. We explain these conductance trends by analyzing the impact of the edge states in these 1D systems on the single-molecule junction transmission. Additionally, we discuss how the self-energy from the electrode-molecule coupling and the on-site energy of the edge sites can be tuned to create longer wires with reversed conductance decays.

KEYWORDS: single-molecule junction, reversed conductance decay, one-dimensional topological insulator, tight-binding, on-site energy

Most molecular wires conducting through an off-resonant transport mechanism exhibit an exponentially decreasing conductance (G) with increasing molecular length (L),[1-5] showing

$$G = G_C e^{-\beta L} \quad (\beta > 0) \tag{1}$$

where β is the exponential decay factor, and G_C is the contact conductance, which depends primarily on the electrode-molecule coupling. According to equation (1), the molecular conductance for a long molecule is inevitably lower than its shorter analogs. This makes it challenging to build long and highly conducting molecular wires. However, researchers have proposed[6-11] and experimentally realized[12-16] a reversed conductance-length decay in mixed-valence or diradical molecular systems, where the conductance increases exponentially with molecular length. Diradical molecules have also been identified as one-dimensional analogs of topological insulators[17], which suggests that this anomalous conductance-length relationship for diradicals is a consequence of their nontrivial topology.[18, 19] By defying exponential decay (equation 1), these molecular systems could inspire the design of long, highly conducting molecular wires.

Interest in diradicals as conductive molecular wires has been motivated by theoretical tight-binding models of polyacetylene in its diradical form. The anomalous conductance-length relationship of diradical polyacetylene was first noted by Hush[20] in the context donor-bridge-acceptor systems and has been popularized more recently by Hoffmann and coworkers[9] in the context of molecular junctions. In these works, the molecule-electrode coupling is neglected, and the conductance of diradical polyacetylene is predicted to increase exponentially with length (i.e., $\beta < 0$). However, since the conductance through a single channel cannot exceed 1 G_0 ($2e^2/h$, the conductance quantum), the conductance cannot exponentially increase indefinitely. As the chain length grows, the molecule-electrode coupling becomes increasingly important. Eventually a long-chain regime is reached where the conductance-length relationship reverts to exponential decay (equation 1), as indicated by the complex band theory[21-23]. This transition between the two conductance-length regimes has recently been shown in experiments[13, 24]. Here, we examine systems of molecular wires terminated by radicals in molecular junctions and use a tight-binding approach[25] to investigate the full evolution of the conductance with length. We further explain how the molecule-electrode coupling and the on-site energy of the edge sites affect the conductance trends, to highlight the role of the electrode-molecule interaction on electron transmission.

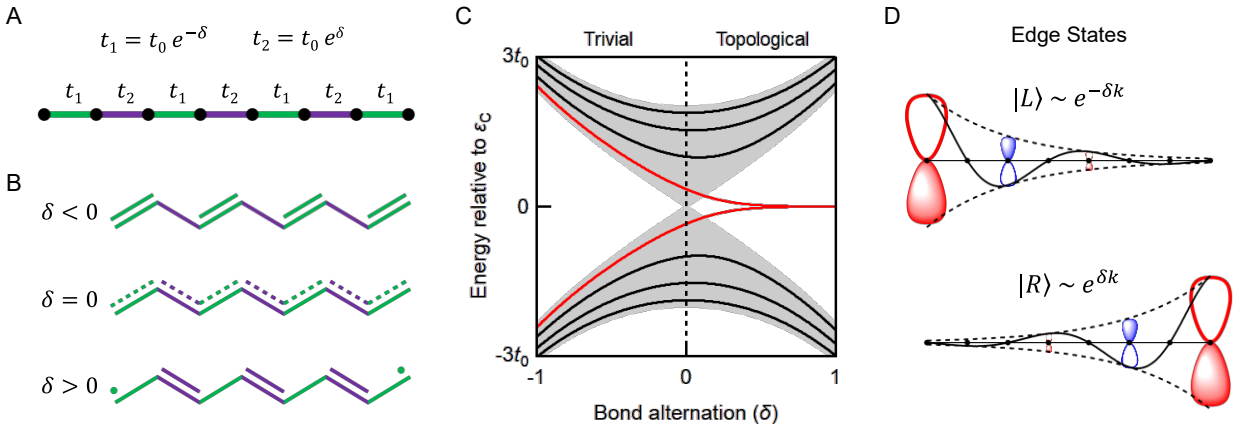

Figure 1. (A) Pictorial depiction of $\mathbf{H}_4$*, which describes a chain of 8 carbon atoms with alternating coupling (*t_1*, green;* t_2*, purple). Alternating coupling is parameterized by* δ*. (B) Chemical interpretation of* δ *in terms of carbon-carbon bond order. For* $\delta < 0$*,* t_1 *represents a double bond and* t_2 *a single bond; whereas, for* $\delta > 0$*,* t_1 *represents a single bond and* t_2 *a double bond. (C) Energy spectrum of* $\mathbf{H}_4$ *as functions of* δ*. The energy bands of the corresponding infinite chain are shaded gray. When* $\delta > 0$*, two edge states (red) exist within the band gap. (D) Schematic molecular orbitals of the left (L) and right (R) edge states for* $m = 4$ *and* $\delta = 0.5$*.*

We first consider the tight-binding model of polyene (i.e., the Su-Schrieffer-Heeger (SSH) model[26, 27] in physics parlance, see SI section 1), and we provide a complete, analytical analysis of the conductance-length relationship. Polyacetylene comprises a chain of sp^2-hybridized carbon atoms that are bonded together by alternating single and double bonds. A simple tight binding model of polyacetylene utilizes two nearest-neighbor coupling parameters, t_1 and t_2, to model the alternating bond orders in the chain. Without loss of generality, the coupling parameters can be expressed by $t_1 = t_0 e^{-\delta}$ and $t_2 = t_0 e^{\delta}$, where t_0 is the geometric mean of t_1 and t_2, and δ parametrizes the bond order alternation. With this parameterization, the Hamiltonian for the SSH model ($\mathbf{H}_m$) is given by equation (2), where m denotes the number of C-C unit cells (Figure 1A). Here we assume $t_1, t_2 > 0$ and a minus sign is included in equation (2) so that the nearest-neighbor coupling is negative. Additionally, we have assigned the on-site energy of the carbon atoms (ε_C) a value of zero. In matrix form, $\mathbf{H}_m$ forms a tridiagonal matrix.

$$\mathbf{H}_m = \sum_{k=1}^{2m-1} -t_0 e^{(-1)^k \delta} |k\rangle\langle k+1| + H.c. \qquad (2)$$

The influence of bond order alternation (δ) on the electronic structure of polyacetylene molecules can be understood from simple Kekulé structures (Figure 1B). When $\delta < 0$, then $t_1 > t_2$ and the molecule assumes the form of a polyene, whereas when $\delta > 0$ then $t_1 < t_2$ and the molecule is a diradical. These two regimes are separated by the condition $\delta = 0$ which describes a chain with uniform bond order ($t_1 = t_2$).

The energy spectrum of $\mathbf{H}_4$ is shown in Figure 1C as a function of δ. It has been shown that $\delta < 0$ and $\delta > 0$ represent two distinct topological classes with trivial and nontrivial topology, respectively. Transitioning from the trivial to the topological regimes requires passing through a gapless metallic state ($\delta = 0$), which demarcates the two topological classes. In the trivial regime ($\delta < 0$), all the energy levels fall within the energy bands of the bulk chain (gray shaded region). In the topological regime ($\delta > 0$), two energy levels (highlighted in red) fall within the band gap. These are edge states that are not accounted for in the bulk band structure. When $\delta \gg 1/m$, the edge states are nearly degenerate with energy ε_{C}. As expected from the simple diradical structure (Figure 1B), the edge states are localized on the left and right edges of the chain (Figure 1D), given by equation (3) and (4), respectively. They decay exponentially into the bulk with alternating orbital phase on every other site. C_m represents the MO coefficient of the first site and is set by unit normalization to be $C_m = \sqrt{\frac{1-e^{-4\delta}}{1-e^{-4\delta m}}}$.

$$|L\rangle = C_m \sum_{k=1}^{2m} \cos[(k-1)\pi/2]\, e^{-\delta(k-1)}\, |k\rangle \tag{3}$$

$$|R\rangle = C_m \sum_{k=1}^{2m} \cos[(k-2m)\pi/2]\, e^{\delta(k-2m)}\, |k\rangle \tag{4}$$

To investigate the electron transmission behavior of polyacetylene, we couple the molecule to electrodes to determine the transmission through the resulting molecular junctions[28-31] (see SI section 2). The molecular junction can be modelled by considering the matrix,

$$\widetilde{\mathbf{H}}_m = \mathbf{H}_m - \frac{i}{2}(\mathbf{\Gamma}_{\mathrm{L}} + \mathbf{\Gamma}_{\mathrm{R}}), \tag{5}$$

where $\mathbf{\Gamma}_{\mathrm{L}} = \Gamma_{\mathrm{L}}|1\rangle\langle 1|$ and $\mathbf{\Gamma}_{\mathrm{R}} = \Gamma_{\mathrm{R}}|2m\rangle\langle 2m|$ are coupling matrices that describe the left and right electrodes, which couple to the first and last site on the chain, respectively (Figure 2A). In a

symmetrically coupled junction, $\Gamma_L = \Gamma_R \equiv \Gamma$. Here we assume the wide-band limit, where the coupling strength, Γ, is independent of energy. From equation (5), the transmission function can be calculated by $T(E) = \mathrm{Tr}[\mathbf{\Gamma}_L \mathbf{G}(E) \mathbf{\Gamma}_R \mathbf{G}^{\dagger}(E)]$, where $\mathbf{G}(E) = \left[E\mathbf{I} - \widetilde{\mathbf{H}}_n\right]^{-1}$ is the Green's function and $\mathbf{I}$ is the identity matrix. At low bias, the conductance of a molecular junction is directly proportional to the transmission at the Fermi energy (E_F): $G = G_0 T(E_F)$ Therefore, we are primarily interested in $T(E_F)$, and for convenience we will assume that $E_F = \varepsilon_C$ (i.e., the carbon on-site energy).

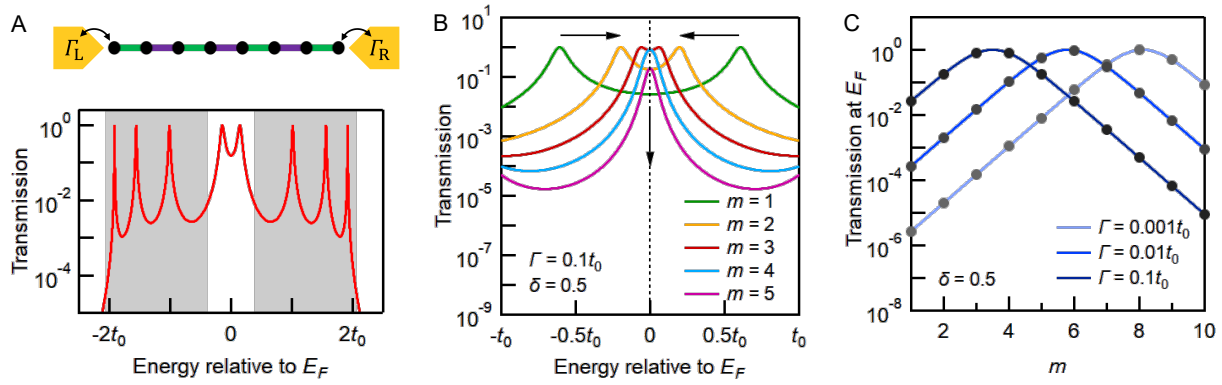

Figure 2. (A) Transmission spectrum for $m = 4$, $\delta = 0.2$, and $\Gamma = 0.1t_0$. The energy bands of an infinite chain are shaded gray. Two resonance peaks exist within the band gap due to the edge states. (B) Transmission spectrum, plotted within the band gap region, for $m = 1$-5 with $\delta = 0.5$, and $\Gamma = 0.1t_0$, Fermi level (E_F) is indicated by the dashed line. (C) Transmission at E_F as a function of length from panel B for $\Gamma = 0.1t_0$, $0.01t_0$, and $0.001t_0$. Short and long chains exhibit exponentially increasing and decreasing transmission, respectively. Grey data points mark the transmission at integer m values.

The transmission function for a representative molecule in the topological regime ($\delta > 0$) is presented in Figure 2A. The transmission function reveals two resonance peaks within the band gap that arise from the edge states. The resonance peaks result in a high transmission at E_F. This suggests that diradical molecules, if chemically stable, serve as good conductors in molecular junctions. The length-dependence of the chain is especially interesting. In Figure 2B, we show the length-dependent transmission near E_F for a chain with $\delta = 0.5$ and $\Gamma = 0.1t_0$. Increasing the length of the chain from $m = 1$ to $m = 3$ causes the edge state-derived resonances to converge to E_F resulting in an increase in $T(E_F)$. This increase in conductance with length is the opposite of

conventional molecular junctions where the conductance decreases exponentially with length (equation (1)). When $m = 4$, for the parameters chosen, the resonance peaks are nearly degenerate and $T(E_F) \approx 1$. However, increasing the length beyond $m = 4$ results in a decrease in $T(E_F)$.

In Figure 2C, $T(E_F)$ is plotted as a function of length (m), using a constant length-independent bond alternation (δ). $T(E_F)$ obeys a simple expression[12] (see SI section 4),

$$T_m(E_F) = \mathrm{sech}^2\left[(2m-1)\delta + \ln\left(\frac{\Gamma}{2t_0}\right)\right] \quad (6)$$

The $\mathrm{sech}^2(x)$ function describes a peak that ranges from zero to one (similar to a Gaussian function). Since δ is the coefficient of m it will primarily affect the width of the peak, while Γ is part of an additive constant that will shift the peak left or right. Restricting our attention to $\delta > 0$ as in the diradical case, since $\Gamma \ll t_0$ in the weak coupling regime, the peak will be centered at some positive m (Figure 2C). However, it should be noted that $T_m(E_F)$ is only meaningful for integer *m* (grey data points), and the peak position of the function will generally not coincide with an integer value. For this reason, the peak conductance of a diradical polyacetylene series will not perfectly reach $1G_0$. Away from the peak center, the transmission exhibits an exponential dependence on length, i.e., $T_m(E_F) \sim e^{-\beta m}$. For short chain lengths $\beta = -4\delta$ and for long chain lengths $\beta = 4\delta$ (see SI section 4). Therefore, although these wires are one-dimensional analogs to 2D and 3D TIs, in that conduction occurs through boundary states, unlike 2D and 3D TI materials, a long chain, which would constitute a 1D material, is conductive at the edge points but not through the entire chain. Only short chains, i.e., small molecules, are conductive via the edge states.

Figure 2C also shows how decreasing Γ affects $T_m(E_F)$. When Γ becomes smaller, $T_1(E_F)$ becomes lower for small *m* and the peak of $T_m(E_F)$ shifts to longer chain lengths since the $\ln(\Gamma/2t_0)$ term becomes more negative. Going from $\Gamma = 0.1t_0$ to $\Gamma = 0.01t_0$ and $0.001t_0$, the chain length with peak transmission increases from *m* = 3 to *m* = 6 and *m* = 8.[32] Accordingly, to extend the range of *m* where we have a negative decay to create longer highly conducting wires, it is necessary to efficiently decouple the polyacetylene chain from the electrodes.

To gain greater intuition on how the edge states mediate transmission it is instructive to consider an explicit two-level model. The left and right edge states presented in equation (3) and (4) are exact eigenstates for infinite chains with energy $\varepsilon_C = 0$. However, for finite chains, $|L\rangle$ and

$|R\rangle$ are no longer eigenstates, but they serve as an effective basis to approximate the HOMO and LUMO of $\mathbf{H}_m$. Applying equation (3) and (4) to equation (2), the coupling between $|L\rangle$ and $|R\rangle$ can be calculated to be:

$$\varepsilon = \langle L|\mathbf{H}_m|R\rangle = (-1)^m|C_m|^2 t_0 e^{-\delta(2m-1)} \tag{7}$$

The coupling between $|L\rangle$ and $|R\rangle$ results in eigenstates that are the symmetric and antisymmetric linear combinations of $|L\rangle$ and $|R\rangle$ with energies $+\varepsilon$ and $-\varepsilon$, respectively. When m = odd, since $\varepsilon < 0$ (equation (7)), the symmetric combination will be lower in energy and become HOMO (i.e., $|\psi_{\mathrm{HOMO}}\rangle$) and the antisymmetric linear combination will be higher in energy (i.e., $|\psi_{\mathrm{LUMO}}\rangle$). When m = even, since $\varepsilon > 0$ (equation (7)), the HOMO and LUMO become reversed:

$$|\psi_{\mathrm{HOMO}}\rangle = \frac{1}{\sqrt{2}}(|L\rangle - (-1)^m|R\rangle), \qquad E_{\mathrm{HOMO}} = -|\varepsilon| \tag{8}$$

$$|\psi_{\mathrm{LUMO}}\rangle = \frac{1}{\sqrt{2}}(|L\rangle + (-1)^m|R\rangle), \qquad E_{\mathrm{LUMO}} = |\varepsilon| \tag{9}$$

The electrode coupling is given by the atomic orbital-electrode coupling (Γ) times the magnitude squared of the MO coefficient at the contact site. The MO coefficient of the electrode contact site for both the HOMO and LUMO is $C_m/\sqrt{2}$ (equation (8) and equation (9)). Therefore, the electrode coupling for both the HOMO and the LUMO is the same and is given by,

$$\gamma = \frac{1}{2}|C_m|^2\Gamma \tag{10}$$

With the energy levels ($\pm\varepsilon$) and the electrode coupling (γ), the transmission coefficients for the HOMO and LUMO are given by the Breit-Wigner formula[33-35] (see SI section 3),

$$t_{\mathrm{HOMO}} = \frac{(-1)^{m-1}\gamma}{E + \varepsilon + i\gamma} \tag{11}$$

$$t_{\mathrm{LUMO}} = \frac{(-1)^m\gamma}{E - \varepsilon + i\gamma} \tag{12}$$

According to equation (11) and (12), the phase of HOMO (or LUMO) alternates from 0 (or π) to π (or 0) for odd and even m. The transmission function for the two-level model is given as the magnitude squared of the sum of transmission coefficients,

$$T_m^{(2)}(E) = |t_{\mathrm{HOMO}} + t_{\mathrm{LUMO}}|^2 \tag{13}$$

The two-level transmission function for a representative molecule ($m = 4$, $\delta = 0.2$, and $\Gamma = 0.1t_0$) is presented in Figure 3A. Due to quantum interference the transmission function (solid) is not a simple sum of the single level Lorentzians (dashed) (see SI section 3). The energy splitting between the resonance peaks is $\Delta E = 2\varepsilon$ and the full width at half maximum (FWHM) for each resonance is 2γ.

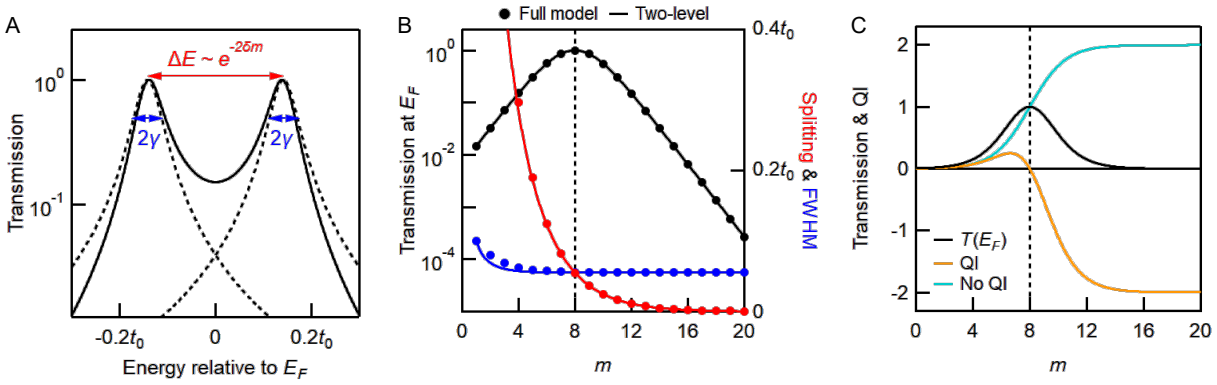

Figure 3. (A) Transmission function for two-level model of edge states (black) along with hypothetical transmission for the individual levels (dashed). The energy splitting and the FWHM of the HOMO/LUMO are indicated by blue and red arrows, respectively. (B) Comparison of the length dependence of transmission (left axis) to the energy splitting (right axis, red) and the FWHM (right axis, blue). The peak in the transmission versus m occurs when the energy splitting equals the FWHM (vertical dashed line). There is good agreement between the full model ($\tilde{\mathbf{H}}_m$) and the two-level model. (C) Transmission from panel B, now plotted on a linear scale, along with the interfering (orange) and noninterfering (blue) terms. The peak transmission occurs when QI is zero.

The transmission at E_F for the two-level model is given by equation (14). Remarkably, equation (14) is equivalent to equation (6), which was derived from the full Hamiltonian, i.e., $T_m^{(2)}(E_F) = T_m(E_F)$. This equivalence with the full model underscores the validity of the two-level approximation. In Figure 3B, $T_m^{(2)}(E_F)$ (black line) is compared with the length dependence of the level splitting ($\Delta E = 2\varepsilon$, red line) and the FWHM (2γ, blue line), with $\delta = 0.2$, and $\Gamma = 0.1t_0$. The level splitting and FWHM from the full model are included as markers. For the full model, the splitting and FWHM are extracted from real and imaginary parts of the eigenvalues of $\tilde{\mathbf{H}}_m$

(equation (5)), which take the form of $\varepsilon - i\gamma$. There is very good agreement between the full model and the two-level model. Importantly, Figure 3B demonstrates that peak transmission at E_F occurs when the splitting equals the FWHM ($\Delta E = 2\gamma$). This condition is analogous to the Rayleigh criterion from optics. Hence, for $\Delta E \gg 2\gamma$ transmission increases exponentially with length, whereas, for $\Delta E \ll 2\gamma$ transmission decreases exponentially with length.

$$T_m^{(2)}(E_F) = \left| \frac{(-1)^{m-1}\,\Gamma/2}{t_0 e^{-(2m-1)\delta} + i\,\Gamma/2} + \frac{(-1)^{m}\,\Gamma/2}{-t_0 e^{-(2m-1)\delta} + i\,\Gamma/2} \right|^2 \tag{14}$$

The condition that $T_m(E_F) = 1$ when $\Delta E = 2\gamma$ is an intuitive result. Each Lorentzian peak contributes 0.5 to transmission resulting a total transmission of 1. However, this argument is only true if the quantum interference (QI) is zero.[36] $T_m^{(2)}(E_F)$ can be expanded into a noninterfering term ($|t_{\mathrm{HOMO}}|^2 + |t_{\mathrm{LUMO}}|^2$) and an interfering term ($2\mathrm{Re}[t_{\mathrm{HOMO}} t_{\mathrm{LUMO}}^*]$). These terms are plotted alongside the transmission function in Figure 3C. When transmission is peaked at 1, indeed QI is zero. For shorter chains, when $\Delta E \gg 2\gamma$, there is constructive interference between the HOMO and LUMO, as expected from the Yoshizawa rules[37]. For longer chains, when $\Delta E \ll 2\gamma$, there is destructive interference, and in the infinite chain limit the HOMO and LUMO coincide in energy and have opposite phase, resulting in complete destructive interference. Equivalently, instead of considering QI between MOs, for long chains one can consider that the basis states, $|L\rangle$ and $|R\rangle$, are too weakly coupled (equation (7)) to facilitate transmission.

We next consider a related system in which the polyacetylene backbone is terminated by two non-carbon atoms, X, as such systems better model real molecular systems that can be probed experimentally through single molecule measurements. For example, X could be a terminal linker such as $–NH_2$ or $–SCH_3$.[38] The onsite energy for X, ε_{X}, will be different from that of carbon and hence non-zero (Figure 4A). This energy offset, as well as its magnitude relative to $\Gamma_{\mathrm{L/R}}$, influences the transmission function.

In the new system including a non-carbon terminal group, the Hamiltonian becomes

$$\widetilde{\mathbf{H}}'_m = \left(\varepsilon_{\mathrm{X}} - \frac{i\Gamma_L}{2}\right)|1\rangle\langle 1| + \left(\varepsilon_{\mathrm{X}} - \frac{i\Gamma_R}{2}\right)|2m\rangle\langle 2m| + \mathbf{H}_m \tag{15}$$

With $\Gamma_L = \Gamma_R \equiv \Gamma$, and $E_F = \varepsilon_{\mathrm{C}} = 0$, we can derive the transmission at Fermi, $T'_m(E_F)$ as was done above for the simple polyacetylene (see SI Section 5). Since $T'_m(E_F)$ is an even function with

respect to ε_X (SI Figure S3), in the discussion below ε_X is set to be positive without loss of generality. Similar to equation (14), we can also consider contributions to transmission from just the two edge states and rewrite $T'_m(E_F)$ as:

$$T_m'^{(2)}(E_F) = \left| \frac{(-1)^{m-1}\,\Gamma/2}{-\varepsilon_X + t_0 e^{(N-1)\delta} + i\,\Gamma/2} + \frac{(-1)^{m}\,\Gamma/2}{-\varepsilon_X - t_0 e^{(N-1)\delta} + i\,\Gamma/2} \right|^2 \qquad (16)$$

Compared with the all-carbon polyacetylene model (or equivalently when $\varepsilon_X = 0$), the energies of the HOMO and LUMO resonances are shifted up by ε_X while the coupling between the electrode and the HOMO and LUMO levels is still $\Gamma/2$.

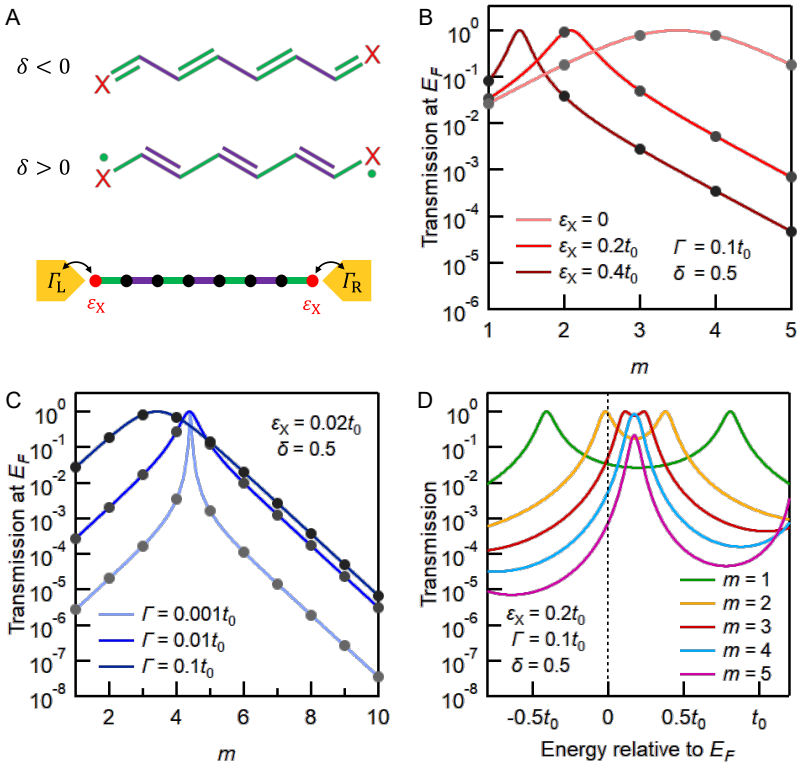

Figure 4. (A) Pictorial depiction of isolated $\mathbf{H}'_4$*, and* $\widetilde{\mathbf{H}}'_4$ *with terminal non-carbon atoms X which have on-site energy* $\varepsilon_X \neq 0$*. All the other parameters are the same as those of the all-carbon polyacetylene model. (B) Plots of the transmission at* E_F *as functions of length m, with* ε_X *increasing from 0 to* $0.5t_0$*, while fixing* $\Gamma = 0.1t_0$ *and* $\delta = 0.5$*. (C) Plots of the transmission at* E_F *as functions of length m fixing* $\varepsilon_X = 0.02t_0$ *and* $\delta = 0.5$*, with* $\Gamma = 0.001t_0$*,* $0.01t_0$*, and* $0.1t_0$*. (D) Transmission functions of m = 1-5 for* $\Gamma = 0.1t_0$*,* $\varepsilon_X = 0.2t_0$ *and* $\delta = 0.5$*.*

We plot $T'_m(E_F)$ as a function of m for different values of ε_X in Figure 4B. We can see that the maxima in $T'_m(E_F)$ shift to smaller m as ε_X increases. Since only integer m values are allowed (grey dots in Figure 4B), a reversed conductance decay requires that $|\varepsilon_X| < 0.2t_0$. We show in Figure 4C the impact of the electrode coupling Γ on $T'_m(E_F)$. In the polyacetylene case, smaller Γ shifts the peak of $T_m(E_F)$ to longer chains without changing the peak shape (Figure 2C). However, with non-zero ε_X, the relative energies of ε_X and Γ are important. If $\varepsilon_X \ll \Gamma$ (dark blue), the peak shape is not affected. If $\varepsilon_X \approx \Gamma$ (medium blue) or $\varepsilon_X \gg \Gamma$ (light blue), the peak becomes sharper with the peak position remaining the same, indicating that ε_X becomes the determining factor in the trends of $T'_m(E_F)$ with m while Γ only affects the peak width. As a result, unlike the all-carbon model, there is a limit in decreasing Γ to extend the wire length over which a negative conductance decay will be observed. If Γ approaches ε_X, this will no longer hold.

We then plot the transmission functions, $T'_m(E)$, in Figure 4D for a fixed ε_X and Γ. We see that $E_F = 0$ is not centered between the two resonance peaks derived from the edge states. However, E_F is in the middle of the bulk state-derived resonance peaks since $\varepsilon_C = 0$. Similar to the all-carbon model, as the chain length increases, these edge-state derived resonances get closer and merge into one peak. After the two resonance peaks coalesce, the transmission peak falls below 1 (for m = 5 in Figure 4D) and the system reverts to a conventional wire with exponentially decreasing conductance again because of destructive QI.

We next expand our model to capture a poly-*p*-phenylene wire terminated with non-carbon atoms (X) to explore whether reversed conductance decay can be achieved in synthetically accessible structures.[24] A diradical character emerges when polyphenylene is oxidized to the quinone that can support edge states (Figure 5B). In this system, a single parameter δ is insufficient to probe the structural transition between the quinone form and diradical form because there are effectively three types of C-C bonds as illustrated in Figure 5A and 5B. Thus, we use constants $t_1 = e^{-0.5}t_0$, $t_2 = e^{0.5}t_0$, and $t = 1t_0$ to describe the two resonance structures separately. The Hamiltonians $\widetilde{\mathbf{H}}_{m,q}$ for the quinoidal structure and $\widetilde{\mathbf{H}}_{m,r}$ for the radical structure using m as the number of phenylene units in the chain and ε_X as the on-site energy of the terminal atom are:

$$\widetilde{\mathbf{H}}_{m,q} = \left(\varepsilon_X - \frac{i\Gamma_L}{2}\right)|1\rangle\langle 1| + \left(\varepsilon_X - \frac{i\Gamma_R}{2}\right)|6m+2\rangle\langle 6m+2| - t_1 \sum_{j,k}^{C-C} |j\rangle\langle k| - t_2 \sum_{p,q}^{C=C} |p\rangle\langle q| + H.c. \quad (17)$$

$$\tilde{\mathbf{H}}_{m,r} = \left(\varepsilon_X - \frac{i\Gamma_L}{2}\right)|1\rangle\langle 1| + \left(\varepsilon_X - \frac{i\Gamma_R}{2}\right)|6m+2\rangle\langle 6m+2| - t_1 \sum_{j',k'}^{C-C} |j'\rangle\langle k'| - t \sum_{p',q'}^{C=C} |p'\rangle\langle q'| + H.c. \quad (18)$$

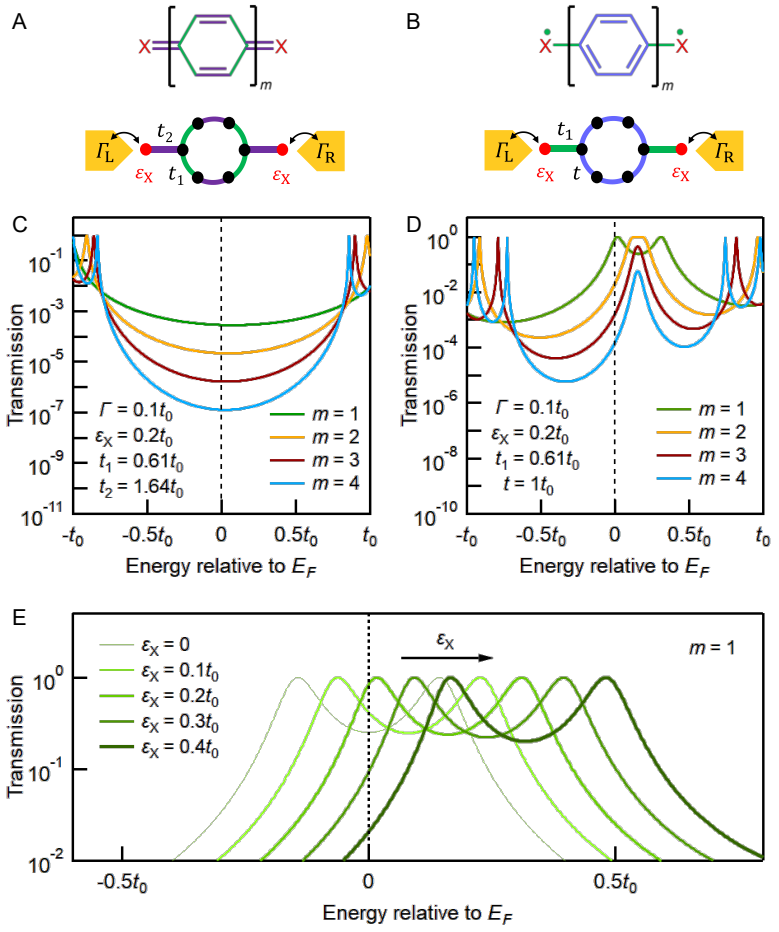

Figure 5. (A) Pictorial depiction of an oxidized poly-p-phenylene chain in the quinoidal form. (B) Pictorial depiction of the same oxidized poly-p-phenylene chain in the diradical form. (C) The calculated transmission function for m = 1-4 for the quinoidal form. (D) The calculated transmission function for m = 1-4 for the diradical form. (E) The evolution of the two edge-state-derived resonance peaks of the diradical poly-p-phenylene with m = 1 and ε_X increasing from 0 to 0.4t_0. For Figures (C)-(E), the Fermi level (E_F, dashed lines) is in the middle of the bulk state-derived resonance peaks.

For $\tilde{\mathbf{H}}_{m,q}$ (equation (17)), we have a sum over the single-bond sites (*j*,*k*) that have a coupling t_1 and double-bond sites (*p*,*q*) that have a coupling t_2. For $\tilde{\mathbf{H}}_{m,r}$ (equation (17)), we have a sum over the inter-phenylene single-bond sites (*j′*,*k′*) with a coupling t_1 and the intra-phenylene

bond sites (p',q') with a coupling t. With $\Gamma_{\mathrm{L}} = \Gamma_{\mathrm{R}} \equiv \Gamma$, the calculated transmissions at E_F, $T_{m,q}(E_F)$ and $T_{m,r}(E_F)$ are derived in SI section 6. Similar to the X-terminated polyacetylene system, we only consider the cases in which ε_{X} is positive.

We plot the full transmission functions of the quinoidal junction in Figure 5C where we see that longer chains have smaller HOMO and LUMO gaps. However, as the orbitals get delocalized over longer lengths as the molecule gets longer, electron density decreases throughout molecular backbone which results in a weaker electrode-molecule coupling. By contrast, for the diradical junction (Figure 5D), we obtain two additional edge state-derived resonance peaks in the middle of the bulk resonance peaks. The transmission function can also be written in a two-level model expression:

$$T_{m,r}^{(2)}(E_F) = \left| \frac{(-1)^{m-1}\,\Gamma/2}{-\varepsilon_{\mathrm{X}} + \tau + i\,\Gamma/2} + \frac{(-1)^{m}\,\Gamma/2}{-\varepsilon_{\mathrm{X}} - \tau + i\,\Gamma/2} \right|^2 \tag{19}$$

where $\tau = t_1^{m+1}/(2t)^m$. Equation (19) shares the same form as equation (16) for the X-terminated polyacetylene system. The two resonance peaks are now separated by $\Delta E = 2\tau$. The plotted transmission functions in Figure 5D are similar to Figure 4D for the X-terminated polyacetylene system. In Figure 5E, we plot the transmission function for m = 1, with increasing ε_{X}. We find that ε_{X} does not affect the shape of the transmission function, but the position of the two resonance peaks relative to E_F. Due to the similarity between this system and the previous polyacetylene systems, the diradical structure of oxidized poly-*p*-phenylene wire can also be classified as a 1D TI. Therefore, this conclusion supports the design of reversed conductance decay in more realistic molecular wires, which has been confirmed in experiments.[24]

We note here that these models and derivations rely on a single-particle approach which does not include electron-electron interactions or the electron spin. In general, electron-electron interactions lead to Coulomb blockade which results in a splitting of the spin-up and spin-down density of states by a charging energy ΔU when one electron occupies a spin-degenerate two-electron level. ΔU (equal to $e^2/C_{\mathrm{junction}}$) is the single-electron charging energy, where e is the charge of an electron and C_{junction} is the capacitance of the junction[39]. At the short chain limit, C_{junction} is small and the Coulomb blockade effect is more significant. Furthermore, introducing non-carbon X atoms at the edges of the polyacetylene or polyphenylene chains could lead to

molecules with net charges. This can give rise to a larger Coulomb blockade effect where the energy for adding one more electron on the molecule is much larger than that indicated by these tight-binding results. Therefore this difference in the charging energy will lead to a larger edge-state HOMO-LUMO gap and E_F will locate between the two edge state resonances.[40] As a result, for the systems with $\varepsilon_X \neq 0$, the reversed conductance decay could extend to longer chains than is be predicted from a tight-binding model.

In conclusion, we incorporate the SSH model with tight-binding transmission calculations to show that 1D wires with topological edge states (topological insulators) can exhibit reversed conductance decay at the short chain limit. According to the two-level model, this reversed conductance decay results from electron transmission mainly through the two topological states which is distinct from the exponential conductance decay that would be obtained from the bulk states. Besides the regular polyacetylene system with an all-carbon backbone, we demonstrate that analogous systems terminated with other atoms also features reverse conductance decay. This work highlights the impact of the topological edge states on the electron transmission. Other factors, such as the electron withdrawing or donating nature of the terminal atoms (ε_X), and the molecular backbone, as well as the molecule-electrodes coupling also affects the electron transmission supported by the edge states, which gives new insights in designing such molecular wires showing reversed conductance decay.

Author information

Corresponding Authors

Suman Gunasekaran − *Department of Chemistry and Chemical Biology, Cornell University, Ithaca, New York 14853, United States; orcid.org/ 0000-0001-5974-0642; Email: sg875@cornell.edu*

Latha Venkataraman − *Department of Chemistry and Department of Applied Physics and Applied Mathematics, Columbia University, New York, New York 10027, United States; orcid.org/0000-0002-6957-6089; Email: lv2117@columbia.edu*

Authors

Liang Li − *Department of Chemistry, Columbia University, New York, New York 10027, United States; orcid.org/ 0000-0003-3890-7276; Email: ll3332@columbia.edu*

Yujing Wei − *Department of Chemistry, Columbia University, New York, New York 10027, United States; orcid.org/0000-0001-8913-9719; Email: yw3557@columbia.edu*

Colin Nuckolls − *Department of Chemistry, Columbia University, New York, New York 10027, United States; orcid.org/0000-0002-0384-5493; Email: cn37@columbia.edu*

Notes

The authors declare no competing financial interests.

Acknowledgements

This research was supported in part by the National Science Foundation under award NSF DMR-1807580 and by the Office of Naval Research under award N00014-20-1-2477. S.G. acknowledges support from the Kavli Institute at Cornell as well as from the American Society for Engineering Education under National Science Foundation grant NSF EEC-2127509.

Reference

(1) Salomon, A.; Cahen, D.; Lindsay, S.; Tomfohr, J.; Engelkes, V. B.; Frisbie, C. D., Comparison of electronic transport measurements on organic molecules, *Adv. Mater.,* **2003,** 15, 1881-1890.

(2) Nitzan, A., Electron transmission through molecules and molecular interfaces, *Annu. Rev. Phys. Chem.,* **2001,** 52, 681-750.

(3) Simmons, J. G., Generalized formula for the electric tunnel effect between similar electrodes separated by a thin insulating film, *J. Appl. Phys.,* **1963,** 34, 1793-1803.

(4) Su, T. A.; Neupane, M.; Steigerwald, M. L.; Venkataraman, L.; Nuckolls, C., Chemical principles of single-molecule electronics, *Nat. Rev. Mater.,* **2016,** 1, 1-15.

(5) Lafferentz, L.; Ample, F.; Yu, H.; Hecht, S.; Joachim, C.; Grill, L., Conductance of a single conjugated polymer as a continuous function of its length, *Science,* **2009,** 323, 1193-1197.

(6) Stuyver, T.; Fias, S.; De Proft, F.; Geerlings, P.; Tsuji, Y.; Hoffmann, R., Enhancing the conductivity of molecular electronic devices, *J. Chem. Phys.,* **2017,** 146, 092310.

(7) Reimers, J.; Hush, N., Electron transfer and energy transfer through bridged systems. I. Formalism, *Chem. Phys.,* **1989,** 134, 323-354.

(8) Joachim, C., Ligand-Length Dependence of the Intramolecular Electron-Transfer through-Bond Coupling Parameter, *Chem. Phys.,* **1987,** 116, 339-349.

(9) Tsuji, Y.; Movassagh, R.; Datta, S.; Hoffmann, R., Exponential Attenuation of Through-Bond Transmission in a Polyene: Theory and Potential Realizations, *ACS Nano,* **2015,** 9, 11109-20.

(10) Li, S. C.; Gan, C. K.; Son, Y. W.; Feng, Y. P.; Quek, S. Y., Anomalous length-independent frontier resonant transmission peaks in armchair graphene nanoribbon molecular wires, *Carbon,* **2014,** 76, 285-291.
(11) Gil-Guerrero, S.; Pena-Gallego, A.; Ramos-Berdullas, N.; Martin Pendas, A.; Mandado, M., Assessing the Reversed Exponential Decay of the Electrical Conductance in Molecular Wires: The Undeniable Effect of Static Electron Correlation, *Nano Lett.,* **2019,** 19, 7394-7399.
(12) Gunasekaran, S.; Hernangomez-Perez, D.; Davydenko, I.; Marder, S.; Evers, F.; Venkataraman, L., Near Length-Independent Conductance in Polymethine Molecular Wires, *Nano Lett.,* **2018,** 18, 6387-6391.
(13) Xu, W., et al., A Peierls Transition in Long Polymethine Molecular Wires: Evolution of Molecular Geometry and Single-Molecule Conductance, *J. Am. Chem. Soc.,* **2021,** 143, 20472-20481.
(14) Zang, Y.; Fu, T.; Zou, Q.; Ng, F.; Li, H.; Steigerwald, M. L.; Nuckolls, C.; Venkataraman, L., Cumulene Wires Display Increasing Conductance with Increasing Length, *Nano Lett.,* **2020,** 20, 8415-8419.
(15) Xu, W., et al., Unusual Length Dependence of the Conductance in Cumulene Molecular Wires, *Angew. Chem. Int. Ed.,* **2019,** 58, 8378-8382.
(16) Leary, E., et al., Bias-driven conductance increase with length in porphyrin tapes, *J. Am. Chem. Soc.,* **2018,** 140, 12877-12883.
(17) Asbóth, J. K.; Oroszlány, L.; Pályi, A., A short course on topological insulators, *Lect. Notes Phys.,* **2016,** 919, 166.
(18) Zhou, Y. X.; Jiang, F.; Chen, H.; Note, R.; Mizuseki, H.; Kawazoe, Y., Quantum length dependence of conductance in oligomers: First-principles calculations, *Phys. Rev. B,* **2007,** 75, 245407.
(19) Stuyver, T.; Zeng, T.; Tsuji, Y.; Geerlings, P.; De Proft, F., Diradical Character as a Guiding Principle for the Insightful Design of Molecular Nanowires with an Increasing Conductance with Length, *Nano Lett.,* **2018,** 18, 7298-7304.
(20) Reimers, J.; Hush, N., Electron transfer and energy transfer through bridged systems III. Tight-binding linkages with zero or non-zero asymptotic band gap, *J. Photochem. Photobiol. A: Chem.,* **1994,** 82, 31-46.

(21) Tomfohr, J. K.; Sankey, O. F., Complex band structure, decay lengths, and Fermi level alignment in simple molecular electronic systems, *Phys. Rev. B,* **2002,** 65, 245105.
(22) Kohn, W., Analytic Properties of Bloch Waves and Wannier Functions, *Phys. Rev.,* **1959,** 115, 809-821.
(23) Jensen, A.; Strange, M.; Smidstrup, S.; Stokbro, K.; Solomon, G. C.; Reuter, M. G., Complex band structure and electronic transmission eigenchannels, *J. Chem. Phys.,* **2017,** 147, 224104.
(24) Li, L., et al., Highly conducting single-molecule topological insulators based on mono- and di-radical cations, *Nat. Chem.,* **2022**.
(25) Atkins, P. W.; Friedman, R. S., *Molecular Quantum Mechanics*. Oxford university press: 2011.
(26) Su, W. P.; Schrieffer, J. R.; Heeger, A. J., Solitons in Polyacetylene, *Phys. Rev. Lett.,* **1979,** 42, 1698-1701.
(27) Heeger, A. J.; Kivelson, S.; Schrieffer, J.; Su, W.-P., Solitons in conducting polymers, *Rev. Mod. Phys.,* **1988,** 60, 781.
(28) Sautet, P.; Joachim, C., Electronic Interference Produced by a Benzene Embedded in a Polyacetylene Chain, *Chem. Phys. Lett.,* **1988,** 153, 511-516.
(29) Sautet, P.; Joachim, C., Electronic transmission coefficient for the single-impurity problem in the scattering-matrix approach, *Phys. Rev. B,* **1988,** 38, 12238-12247.
(30) Mujica, V.; Kemp, M.; Ratner, M. A., Electron conduction in molecular wires. I. A scattering formalism, *J. Chem. Phys.,* **1994,** 101, 6849-6855.
(31) Mujica, V.; Kemp, M.; Ratner, M., Electron conduction in molecular wires. II. Application to scanning tunneling microscopy, *J. Chem. Phys.,* **1994,** 101, 6856-6864.
(32) Gu, M. W.; Peng, H. H.; Chen, I. P.; Chen, C. H., Tuning surface d bands with bimetallic electrodes to facilitate electron transport across molecular junctions, *Nat. Mater.,* **2021,** 20, 658-664.
(33) Breit, G.; Wigner, E., Capture of slow neutrons, *Phys. Rev.,* **1936,** 49, 519.
(34) Schuster, R.; Buks, E.; Heiblum, M.; Mahalu, D.; Umansky, V.; Shtrikman, H., Phase measurement in a quantum dot via a double-slit interference experiment, *Nature,* **1997,** 385, 417-420.

(35) Greenwald, J. E.; Cameron, J.; Findlay, N. J.; Fu, T.; Gunasekaran, S.; Skabara, P. J.; Venkataraman, L., Highly nonlinear transport across single-molecule junctions via destructive quantum interference, *Nat. Nanotechnol.,* **2021,** 16, 313-317.
(36) Gunasekaran, S.; Greenwald, J. E.; Venkataraman, L., Visualizing Quantum Interference in Molecular Junctions, *Nano Lett.,* **2020,** 20, 2843-2848.
(37) Yoshizawa, K., An orbital rule for electron transport in molecules, *Acc. Chem. Res.,* **2012,** 45, 1612-21.
(38) Kamenetska, M.; Koentopp, M.; Whalley, A. C.; Park, Y. S.; Steigerwald, M. L.; Nuckolls, C.; Hybertsen, M. S.; Venkataraman, L., Formation and evolution of single-molecule junctions, *Phys. Rev. Lett.,* **2009,** 102, 126803.
(39) Averin, D. V.; Likharev, K. K., Coulomb Blockade of Single-Electron Tunneling, and Coherent Oscillations in Small Tunnel-Junctions, *J. Low. Temp. Phys.,* **1986,** 62, 345-373.
(40) Datta, S., *Quantum Transport: Atom to Transistor*. Cambridge university press: 2005.